Cell

Disruptive *CHD8* Mutations Define a Subtype of Autism Early in Development

Raphael Bernier,[1,19] Christelle Golzio,[2,19] Bo Xiong,[3,19] Holly A. Stessman,[3,19] Bradley P. Coe,[3,19] Osnat Penn,[3] Kali Witherspoon,[3] Jennifer Gerdts,[1] Carl Baker,[3] Anneke T. Vulto-van Silfhout,[4] Janneke H. Schuurs-Hoeijmakers,[4] Marco Fichera,[5,6] Paolo Bosco,[5] Serafino Buono,[5] Antonino Alberti,[5] Pinella Failla,[5] Hilde Peeters,[7,8] Jean Steyaert,[8,9,10] Lisenka E.L.M. Vissers,[4] Ludmila Francescatto,[2] Heather C. Mefford,[11] Jill A. Rosenfeld,[12] Trygve Bakken,[13] Brian J. O'Roak,[14] Matthew Pawlus,[15] Randall Moon,[15,18] Jay Shendure,[3] David G. Amaral,[16] Ed Lein,[13] Julia Rankin,[17] Corrado Romano,[5] Bert B.A. de Vries,[4] Nicholas Katsanis,[2] and Evan E. Eichler[3,18,*]

[1]Department of Psychiatry, University of Washington, Seattle, WA 98195, USA
[2]Center for Human Disease Modeling, Duke University Medical Center, Durham, NC 27710, USA
[3]Department of Genome Sciences, University of Washington School of Medicine, Seattle, WA 98195, USA
[4]Department of Human Genetics, Radboud University Medical Center, 6525 GA Nijmegen, The Netherlands
[5]I.R.C.C.S. Associazione Oasi Maria Santissima, Troina 94018, Italy
[6]Medical Genetics, University of Catania, Catania 95123, Italy
[7]Center for Human Genetics, University Hospitals Leuven, KU Leuven, 3000 Leuven, Belgium
[8]Leuven Autism Research (LAuRes), 3000 Leuven, Belgium
[9]Department of Child and Adolescent Psychiatry, KU Leuven, 3000 Leuven, Belgium
[10]Department of Clinical Genetics, Academic Hospital Maastricht, and Research Institute Growth & Development (GROW), Maastricht University, 6200 MD Maastricht, The Netherlands
[11]Department of Pediatrics, University of Washington, Seattle, WA 98195, USA
[12]Signature Genomics Laboratories, PerkinElmer, Inc., Spokane, WA 99207, USA
[13]Allen Institute for Brain Science, Seattle, WA 98103, USA
[14]Molecular & Medical Genetics, Oregon Health & Science University (OHSU), Portland, OR 97208, USA
[15]Department of Pharmacology, University of Washington, Seattle, WA 98109, USA
[16]Autism Phenome Project, MIND Institute, University of California-Davis, Sacramento, CA 95817, USA
[17]Peninsula Clinical Genetics Service, Exeter EX1 2ED, UK
[18]Howard Hughes Medical Institute, Seattle, WA 98195, USA
[19]Co-first authors
*Correspondence: eee@gs.washington.edu
http://dx.doi.org/10.1016/j.cell.2014.06.017

SUMMARY

Autism spectrum disorder (ASD) is a heterogeneous disease in which efforts to define subtypes behaviorally have met with limited success. Hypothesizing that genetically based subtype identification may prove more productive, we resequenced the ASD-associated gene *CHD8* in 3,730 children with developmental delay or ASD. We identified a total of 15 independent mutations; no truncating events were identified in 8,792 controls, including 2,289 unaffected siblings. In addition to a high likelihood of an ASD diagnosis among patients bearing *CHD8* mutations, characteristics enriched in this group included macrocephaly, distinct faces, and gastrointestinal complaints. *chd8* disruption in zebrafish recapitulates features of the human phenotype, including increased head size as a result of expansion of the forebrain/midbrain and impairment of gastrointestinal motility due to a reduction in postmitotic enteric neurons. Our findings indicate that *CHD8* disruptions define a distinct ASD subtype and reveal unexpected comorbidities between brain development and enteric innervation.

INTRODUCTION

Autism spectrum disorder (ASD) is a heterogeneous disorder with significant genotypic and phenotypic complexity (Geschwind, 2009). Although various behaviorally defined subtypes have been proposed (American Psychiatric Association, 2000; Wing and Gould, 1979), these have not been tied to genetic etiology, linked to treatment indicators, nor diagnosed consistently by expert clinicians (Lord et al., 2012). Indeed, with the transition to the DSM-5, all behaviorally defined subtypes have been subsumed by the umbrella term autism spectrum disorder, allowing for identification of subtypes more closely aligned to biological mechanisms (American Psychiatric Association, 2013). The genetic etiology of ASD is no less varied. More than 100 genes and genomic regions have been associated with ASD (Betancur, 2011), and >800 genes have been suggested to play a role in

Table 1. Summary of *CHD8* Mutations (from 5′ to 3′)

Proband	Sex	Mutation[b]	HGVS[c]	Diagnosis[d]	Inheritance
12714.p1[a]	M	Ns	p.Ser62X	ASD	de novo
13986.p1[a]	M	Fs	p.Tyr747X	ASD	de novo
Nij023486	F	Fs	p.Val984X	ID/ASD	inherited, maternal
APP_109580-100	M	Ns	p.Glu1114X	ASD	de novo
11654.p1[a]	F	Sp	c.3519-2A > G	ASD	de novo
13844.p1[a]	M	Ns	p.Gln1238X	ASD	de novo
14016.p1[a]	M	Ns	p.Arg1337X	ASD	de novo
Troina2659	M	Fs	p.Glu1932SerfsX3	DD/ID/ASD	de novo
12991.p1[a]	M	Fs	p.Glu2103ArgfsX3	ASD	de novo
12752.p1[a]	F	Fs	p.Leu2120ProfsX13	ASD	de novo
Troina2037	F	Fs	p.Glu2136ArgfsX6	ID	de novo
Nij010878	M	Aa	p.Lys2287 del	ID/ADHD	unknown
14233.p1[a]	M	Fs	p.Asn2371LysfsX2	ASD	de novo
14406.p1[a]	M	Aa	p.His2498 del	ASD	de novo
Gecz4801	M	Mns	p.Arg910Gln	ID?	unknown
Leuven_445853	M	Mns	p.Gly1710Val	ASD	inherited, maternal
Nij07-06646	M	Mns	p.Arg1797Gln	ASD	inherited, paternal
T102.03	F	CNV-dup		ASD	inherited, paternal
9883540		CNV-dup		DD, dysmorphic features	unknown
9873678		CNV-dup		mild ID	unknown

[a]Patient mutation was previously reported (O'Roak et al., 2012b).
[b]Ns, nonsense; Fs, frameshift; Sp, splice; Aa, single amino-acid deletion; Mns, missense-near-splice site; CNV, copy-number variant; dup, duplication.
[c]HGVS, human genome variant sequence.
[d]ASD, autism spectrum disorder; DD, developmental delay; ID, intellectual disability; ADHD, attention deficit hyperactivity disorder.

ASD (Iossifov et al., 2012; Neale et al., 2012; O'Roak et al., 2012b; Sanders et al., 2012). Given that parsing the behavioral heterogeneity has yielded limited utility, genetically defined subtypes may prove more beneficial in illuminating molecular mechanisms underlying ASD, the course and prognosis of a subgroup of individuals with ASD, and individualized treatment targets.

Severe disruptive mutations in chromodomain helicase DNA-binding protein 8 (*CHD8*) have been associated with ASD and provide a likely candidate for a specific subtype of ASD (O'Roak et al., 2012b; Talkowski et al., 2012; Neale et al., 2012). *CHD8*, located on 14q11.2, binds to β-catenin in its function in chromatin remodeling (Thompson et al., 2008) and as a potential regulator of Wnt signaling (Nishiyama et al., 2012). *CHD8* has been associated with rare cases in childhood disorders; two sporadic truncating mutations in autism patients were identified by O'Roak et al. (2012b) from exome sequencing of 209 proband-parent trios from the Simons Simplex Collection (SSC; Fischbach and Lord, 2010). Concurrently, examination of balanced chromosomal abnormalities in individuals with neurodevelopmental disorders reported a novel disruption to *CHD8* in an individual with ASD (Talkowski et al., 2012). Based on these findings, Neale and colleagues performed a case-control analysis and found an excess of disruptive mutations in ASD exomes (three cases) (Neale et al., 2012). Subsequent targeted sequencing using molecular inversion probes (MIPs) in 2,446 individuals from the SSC identified eight individuals with recurrent truncating mutations within *CHD8*, with six of the eight individuals showing evidence of macrocephaly (O'Roak et al., 2012b). Multiple converging reports thus suggest that mutation of *CHD8* is an important risk factor of ASD. The goal of this study was to determine whether *CHD8* mutations define a specific subtype of ASD through the discovery of additional patients, extensive phenotype-genotype correlations, and modeling truncating mutations during zebrafish development.

RESULTS

Patient and Mutation Discovery

Previously, we identified nine de novo mutations in 2,446 probands from the SSC; this included eight putative loss-of-function mutations and one in-frame amino-acid deletion (Table 1). To expand the patient collection and determine the specificity of the phenotype for autism, we targeted a cohort of patients with more broadly defined developmental delay phenotypes. Using MIPs, we resequenced *CHD8* in 3,730 additional children with ASD or developmental delay and validated eight additional potentially disruptive mutations (Table 1 and Figure 1), including three frameshift, one stop-gain, one amino-acid deletion, and three missense-near-splice sites. We first compared our findings of 13 truncating mutations in 6,176 cases to a well-characterized control cohort of 2,289 unaffected siblings from the SSC; we sequenced *CHD8* among the unaffected siblings and found no putative disruptive mutations. This confers a nominally significant case-control p value of $p = 0.0167$ (Fisher's exact test).

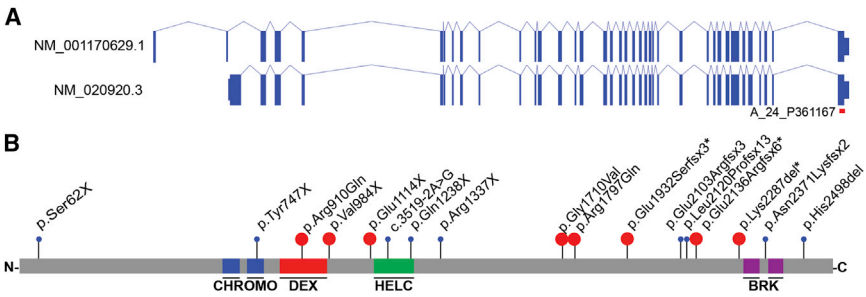

Figure 1. Spectrum of *CHD8* Mutations in Autism Spectrum Disorder

(A and B) (A) Gene isoforms 1 and 2 and (B) protein models of *CHD8* with proband putative disruptive mutations indicated. The location of the gene expression array probe used for Figure 3 (A_24_P361167) is shown in (A) in red. Events in blue were reported previously (Neale et al., 2012; O'Roak et al., 2012a). Events in red are novel. (*) Diagnosis of intellectual disability (Table 1). See also Tables S1 and S2 and Figure S1.

To expand our analysis, we incorporated an additional 6,503 general population controls from the Exome Sequencing Project (http://evs.gs.washington.edu/EVS/). Although not screened specifically for neuropsychiatric conditions, we again observed no additional truncating events in *CHD8*. Taking these two control populations together, we refined our estimate of significance for *CHD8* truncation to $p = 1.01 \times 10^{-5}$ (Fisher's exact test, odds ratio is infinite, with a 95% C.I. from 4.34 to infinity) (Table S1).

The majority of truncating mutations (nonsense, frameshift, and canonical splice site) for which inheritance could be determined were de novo (11 of 12 (92%) with cascade screening; Figure 1 and Table 1). Complementary to our case-control analysis, we applied a probabilistic model derived from human-chimpanzee fixed difference and sequence context, as described in O'Roak et al. (2012a), to calculate the null probability of the *CHD8* truncating variation. Under a de novo rate of 1.2 nonsynonymous coding variants per individual, we estimate the probability of detecting 11 or more *CHD8* de novo truncating events in 6,176 cases as $p = 9.4 \times 10^{-23}$ (binomial test). This is significant in that this probability exceeds even a strict exome-wide significance cutoff of 2.5×10^{-6} assuming that we had screened all 20,000 genes. Two missense-near splice sites and a 5 kbp copy-number duplication in the carboxy terminus of the gene were found to be inherited (Figure S1 available online and Table 1).

No copy-number variants (CNVs) were observed across this locus in 19,584 population controls. Four variants were detected near canonical splice sites of *CHD8* (three missense: Nij07-06646, Leuven445853, and Gecz4801 and one intronic: 11654.p1). Using Alamut 2.3 (Interactive Biosoftware), we assessed the likely impact of each mutation on splicing (Houdayer, 2011). One variant (11654.p1) disrupts the intronic canonical splice acceptor signal and likely disrupts splicing (Figure 1B and Table S2). Three additional variants were located in the exonic sequence and represent missense-near splice variation. One of these (Nij07-06646) affects the last base of the exon and is predicted to abrogate significantly the local splice site (Figure 1B and Table S2), whereas the other two (Leuven445853 and Gecz4801) are located two bases in from the splice junction and are not predicted to be disruptive (Figure 1B and Table S2). In this regard, the two cases predicted to have the most severe canonical splice-site disruptions exhibit the characteristic features associated with *CHD8* putative disruptive mutations, whereas the two variants that do not likely disrupt splicing were inherited (Tables 2 and S5). The less severe event from Leuven445853 is milder in its presentation. We also found that milder mutations were more likely to be inherited from unaffected parents. Cascade testing showed that the only inherited severe mutation (Nij07-06646) was transmitted from a father who demonstrated similar behavioral challenges related to autism, had a large head circumference, and experienced recurrent sleeping and gastrointestinal (GI) difficulties.

Clinical Phenotype

We recontacted eight *CHD8* patients and their families for structured clinical assessment, review of medical records, and dysmorphological evaluation (Figure 2). This included three families from the SSC (O'Roak et al., 2012b) as well as five newly discovered patients identified by MIP screening of patients with ASD and developmental delay. We integrated these findings and generated clinical reports for all available families, yielding a phenotypic description of 15 patients from individuals with potentially disruptive mutations (Tables 2 and Table S5).

ASD was the most common diagnosis observed in our cohort. Of the 15 identified individuals evaluated, 13 meet strict diagnostic criteria for ASD; 1 is an adult suspected of having a psychotic disorder, and 1 is diagnosed with ADHD and borderline intellectual functioning. Of the 9 children who underwent a formal, standardized ASD evaluation using gold standard diagnostic instruments, all met criteria for autistic disorder on both the ADOS and ADI. ASD severity, as measured with the calibrated severity score (Gotham et al., 2009), fell within the diagnostic realm (mean CSS = 6.8, SD = 1.3), underscoring the confidence of the diagnosis. Even among patients referred only for developmental delay, follow-up showed that most had ASD or ASD symptoms (Table 1). Altogether, at least 87% and possibly 93% have a diagnosis of ASD, providing evidence that disruptive mutations to *CHD8* are heavily enriched and possibly specific to ASD.

Although patients varied in age from 4 to 41 years of age, we observed striking similarities in their facial characteristics (Figure 2A). Predominant features included increased occipitofrontal circumference (OFC), pronounced supraorbital brow ridges, wide-set eyes with down-slanted palpebral fissures, broad nose with full nasal tip, and pointed chin. Other recurrent physical features included slender, tall build and large, flat feet, which have been reported in several individuals (Table S5). 80% of the cases have macrocephaly (OFC $z > 2.0$) either at the time of testing or earlier in development. The observed rate of macrocephaly in this case series cohort is significantly greater (Fisher's exact test, $p = 2.1 \times 10^{-8}$) than that observed in children with ASD from the SSC without *CHD8* mutations (360/2,564 or

Table 2. Brief Description of Phenotypic Presentation of 15 Patients with *CHD8*-Truncating Single-Nucleotide Variants

Patient	12714.p1	13986.p1	Nij023486	APP_09580 – 100	11654.p1	13844.p1	14016.p1	Troina2659	12991.p1	12752.p1	Troina2037	Nij – 010878	14233.p1	14406.p1	Nij07 – 06646	Observed N (% of Sample)
Sex	M	M	F	M	F	M	M	M	M	F	F	M	M	M	M	
Age at testing (years)	4	5	15	6	12	8	8	13	16	4	41	11	16	13	17	
Macrocephaly	–	+	+	+	+	+	+	+	+	+	+	–	+	–	+	12 (80%)
Prominent supraorbital ridge	u	u	+	–	+	u	+	+	+	u	+	–	u	u	+	7/9 (78%)
Hypertelorism	u	u	+	+	+	u	+	–	+	u	+	–	u	u	–	6/9 (67%)
Down-slanted palpebral fissures	u	u	+	–	+	u	+	+	–	u	+	–	u	u	+	6/9 (67%)
Flat feet	u	u	–	–	–	u	–	–	+	u	–	–	u	u	+	2/9 (22%)
Tall	+	+	+	+	+	+	+	+	–	u	–	+	+	+	+	12/14 (86%)
Overweight	–	–		–	–	–	–	–	–	u	+	+	–	+	–	3/14 (21%)
ASD	+	+	+	+	+	+	+	+	+	+	–	–	+	+	+	13 (87%)
Intellectual disability	–	+	+	+	+	+	–	+	+	–	+	–	+	–	–	9 (60%)
Attentional problems	–	–	+	+	+	–	–	–	+	+	+	+	+	+	–	9 (60%)
Anxiety problems	+	–	–	–	–	–	+	–	+	+	–	–	–	–	–	4 (27%)
Seizures	–	–	–	–	+	–	+	–	+	–	–	–	–	–	–	3 (20%)
Regression	+	–	+	+	+	+	–	+	–	–	–	–	+	–	–	7 (47%)
GI problems	+	–	+	+	+	+	+	+	+	+	+	–	+	–	+	12 (80%)
Sleep problems	–	+	+	+	+	–	+	–	+	+	–	–	+	+	+	10 (67%)
C section	–	–	–	–	+	–	–	+	+	+	–	–	–	–	+	5 (33%)
Birth induction/ augmentation	+	+	–	–	+	–	+	–	+	–	–	–	–	+	–	6 (40%)

+, present; –, absent; u, unknown. Detailed phenotypic data are outlined for each patient in the above domains in Table S5. Where a denominator is indicated, unknown values were excluded from the percent of sample calculation.

14%). The use of reference samples has generated discussions regarding the utility of these data for establishing individual OFC standard scores (Chaste et al., 2013). Certain factors are important to consider when determining the relative head size of individuals. In this case series, larger head size in comparison to individuals with ASD in the SSC without *CHD8* mutations appears independent of height, age, and mean parental head circumference, $F(1, 2639) = 4.79$, $p = 0.029$, Cohen's $d = 3.10$ (large effect size based on estimated marginal means).

We obtained head circumference velocity data for two patients (Figure 2B). The trajectories are characterized by marked early orbital frontal head growth in the first 2 months post birth, followed by consistent large head growth remaining at or above the 97th percentile throughout early childhood, thereby underscoring the penetrance of this aspect of the *CHD8* phenotype. Potentially related, certain patterns emerged in this case series regarding the birth and delivery process. Induction and augmentation of labor is noted in six patients (40%), and C sections were common, with five (33%) reported C section births.

Twelve patients (80%) reported significant GI problems, with 60% reporting specific difficulties characterized as recurrent and consistent problems with constipation. Caregivers often reported long periods of GI disturbance characterized by periods of considerable constipation followed by loose stool or diarrhea. The rate of parent-reported constipation in this case series is significantly greater (Fisher's exact test, $p = 0.006$) relative to parent reports of constipation in children with ASD without *CHD8* mutations from the SSC. Parents of 693 of 2,630 children without *CHD8* mutations in the SSC reported problems with constipation (26%) as compared to the 60% rate observed in this cohort.

Sleep problems were reported frequently. Ten patients (67%) reported some type of sleep problem, with seven (44%) presenting specifically with difficulties in falling asleep. Two patients reported sleep challenges so profound that the children would remain awake for days without sleeping. However, this rate is not yet greater than ASD children without *CHD8* mutations (60%; Fisher's exact test, $p = 0.75$), and there is some evidence that this aspect ameliorates with age. Another recurrent

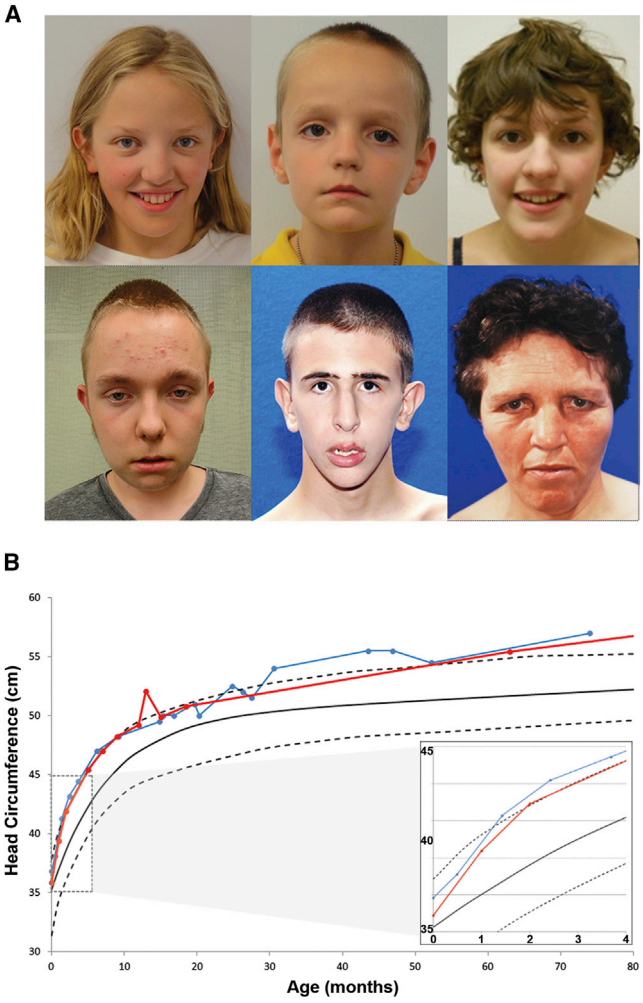

Figure 2. Physical Characteristics of the *CHD8* Phenotype

(A) Facial phenotype associated with *CHD8*. Patients 11654.p1 (upper-left), 14016.p1 (top-middle), and Nij023486 (upper-right) present with macrocephaly, hypertelorism, down-slanted palpebral fissures, broad nose, pointed chin, and broad forehead with prominent supraorbital ridge. Patient 12991.p1 (lower-left) has a high forehead, hypertelorism, large ears, fleshy earlobes, and a history of macrocephaly (at 12 years of age). Patient Troina2659 (bottom-middle) did not have hypertelorism but did present with macrocephaly, down-slanted palpebral fissures, prominent supraorbital ridge, and pointed chin. Additional physical features included posterior plagiocephaly. Patient Troina2037 (lower-right) presented with macrocephaly, hypertelorism, down-slanted palpebral fissures, prominent supraorbital ridges, large ears with fleshy upturned lobes, and full fleshy lips. Additional physical features included widened cranial vault observed via CT scan.

(B) Longitudinal head circumference in *CHD8* patients. Analysis of standardized head circumference values for patients 14016.p1 (in red) and APP_109580-100 (in blue) reveal marked early orbital frontal head growth in the first 2 months post birth followed by consistent large head growth remaining at or above 97th percentile throughout early childhood.

finding is cognitive impairment. Cognitive ability of the cohort ranges from profoundly disabled to age appropriate; however, none of the patients demonstrate an above-average IQ. Nine patients have a comorbid diagnosis of intellectual disability, with each of those children showing impairment in both cognitive and adaptive abilities. Additionally, two of the children manifest cognitive performance in the borderline intellectual functioning range.

CHD8 Expression during Development

Due to its potentially important role during brain development, we determined the spatiotemporal expression profile of *CHD8* based on available microarray and RNA-seq data (Shen et al., 2012). The gene is expressed widely in the adult and developing human and macaque brains (as well as mouse) throughout both cortical and subcortical structures, including the neocortex, hippocampus, amygdala, and striatum (Figures S2, S3A, and S3B). Expression is highest in the early prenatal period (9–16 postconception weeks [pcw]) and decreases during human (Figure 3A) and macaque (Figure S3A) fetal and postnatal development. *CHD8* is also expressed widely across progenitor and postmitotic layers in midfetal human (15–21 pcw) neocortex, with possible enrichment in the intermediate zone at 15 and 16 pcw (Figure 3B), but not at 21 pcw (data not shown). This pattern is in contrast to the known *CHD8*-binding partner *CHD7* (Figure 3A), which is expressed primarily in neural progenitor cell layers (ventricular and subventricular zones; Figure 3C). There is no clear laminar enrichment of *CHD8* in developing macaque cortex (Figure S3B).

We searched for genes with similar temporal patterns of coexpression during human brain development using RNA-seq data obtained from the BrainSpan Atlas (http://www.brainspan.org/). We identified 172 genes with significant coexpression ($r > 0.9$; Figure S2B), of which nine (*SETD2*, *MLL5*, *ADNP*, *POGZ*, *ARID1B*, *PHF2*, *DYRK1A*, *SUV420H1*, *MBD5*) have been reported previously as sites of de novo truncating mutations among ASD probands (Iossifov et al., 2012; Neale et al., 2012; O'Roak et al., 2012a, 2012b; Sanders et al., 2012) (Table S3). The strongest correlation ($r = 0.96$) for *CHD8* was, in fact, a histone methyl transferase, *SETD2*, implicated in epigenetic transcriptional activation and chromatin modulation (Simon et al., 2014). Overall, we find a significant enrichment of autism candidate genes among the *CHD8* coexpressed set ($p = 1.02 \times 10^{-6}$, OR = 9.7, 95% C.I. = 4.3–19.5 for genes $r > 0.9$). This enrichment becomes more pronounced as the correlation threshold is increased ($p = 1.78 \times 10^{-5}$, OR = 83.6, 95% C.I. = 13.4–394.9 at $r > 0.95$; Figures S2C and 3D).

To identify genes coexpressed with *CHD8* specifically in the tissues that appear to be enriched for spatiotemporal expression of *CHD8* (Figure 3B), we performed a tissue-specific coexpression analysis. First, *CHD8* expression was assessed by microarray (Affymetrix probe A_24_P361167; Figure 1A) in each layer of midfetal human (15–21 pcw) neocortex. A total of 282 genes were at least moderately correlated ($r > 0.5$) with *CHD8* expression across all cortical layers. Among them, a total of 144 of 282 genes were also highly correlated ($r > 0.85$) with *CHD8* neocortical expression over time, from the early prenatal period through adulthood. These 144 genes showing elevated prenatal and widespread midfetal laminar expression were associated significantly with chromatin modification and transcription regulation as assessed by gene ontology enrichment (data not shown). Some of the most significantly correlated temporal genes ($r > 0.9$; $p < 1 \times 10^{-16}$; Table S4) include *NAV1*, *MLL*, *ARID1A*,

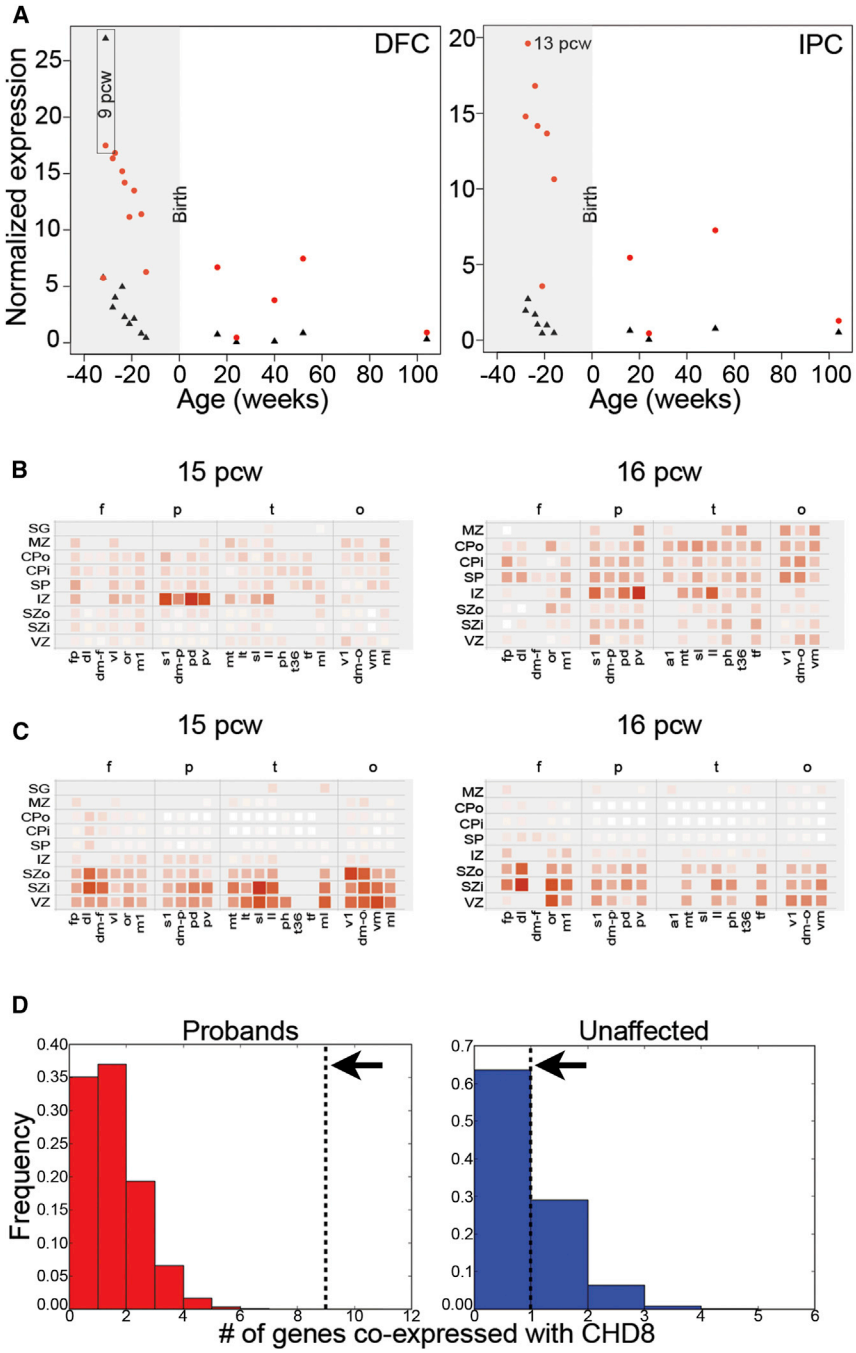

Figure 3. Normal Expression of *CHD8*

(A) Reads per kilobase per million normalized expression values of *CHD8* (red) and *CHD7* (black) in dorsolateral prefrontal cortex (DFC, left) and posteroventral (inferior) parietal cortex (IPC, right) over a range from 8 postconception weeks (pcw) to 104 weeks (2 years) of age taken from normal post autopsy individuals. Highlighted in gray is expression in the fetal brain prior to birth.

(B and C) Heatmap showing localized expression of *CHD8* (B) or *CHD7* (C) at 15 pcw (left) and 16 pcw (right) in the intermediate zone (IZ). Red indicates increased expression, and white indicates no expression. Cortical samples are organized in columns by lobe (f, frontal; p, parietal; t, temporal; o, occipital) and in rows by layer from basal to apical surfaces of the developing neocortex (SG, supragenticulate nucleus of the thalamus; MZ, marginal zone; CPo, outer cortical plate; CPi, inner cortical plate; SP, subplate zone; SZo, outer subventricular zone; SZi, inner subventricular zone; VZ, ventricular zone). Within lobes, samples are approximately ordered from rostral to caudal. a1, primary auditory cortex; dl, dorsolateral prefrontal cortex; dm-f, dorsomedial frontal cortex; dm-o, dorsomedial extrastriate cortex; dm-p, dorsomedial parietal cortex (area 7 m); fp, frontal polar cortex; il, inferolateral temporal cortex; lt, lateral temporal-occipital cortex; m1, posterior frontal cortex (motor cortex); mi-t, midinferior temporal cortex; ml, midlateral extrastriate cortex; mt, medial temporal-occipital cortex; or, orbital frontal cortex; pd, posterosuperior [dorsal] parietal cortex; ph, posterior parahippocampal cortex; pv, posteroinferior [ventral] parietal cortex; s1, primary somatosensory cortex; sl, superolateral temporal cortex; t36, [rostral] midinferior temporal cortex [area 36]; tf, caudal midinferior temporal cortex [area TF]; tp, temporal polar cortex; v1, primary visual cortex; vl, ventrolateral prefrontal cortex; vm, ventromedial extrastriate cortex.

(D) *CHD8* is coexpressed with nine genes carrying truncated mutations in ASD probands (n = 133, red, left) and one gene carrying disruptive mutations in unaffected siblings and controls (n = 58, blue, right) (Gulsuner et al., 2013; Rauch et al., 2012) with Pearson correlation $r > 0.9$ (black dashed lines). For comparison, 100,000 random sets of genes of the same size (n = 133, left; n = 58, right) were sampled. The histogram shows the number of genes from each such random set that are coexpressed with *CHD8*. *CHD8* is found to coexpress with a significantly higher number of genes reported as sites for de novo truncated mutations in ASD probands ($p < 1 \times 10^{-5}$) in contrast to unaffected siblings and controls, which was not significant ($p = 0.37$).

See also Figures S2 and S3 and Tables S3 and S4.

RPRD2, and *ZNF462* (Figure S2D). Of these genes, both *NAV1* and *MLL* have been identified as sites of mutation in ASD probands (Jiang et al., 2013; O'Roak et al., 2012b) (Figure S2B and Table S3).

Zebrafish Modeling

We similarly assessed the pattern of expression of *chd8* during zebrafish development. We designed four antisense probes of ~1.5 kbp each along the length of the gene and assessed expression by in situ hybridization. We found that *chd8* mRNA is maternally deposited into the zygote and expressed ubiquitously until early somitogenesis (Figure 4A). *chd8* mRNA began to show enrichment in the brain and spinal cord at 1 day postfertilization (dpf) and then became progressively restricted to the head and gut regions later during embryonic development at 3–4 dpf. Because the CHD8 protein is highly

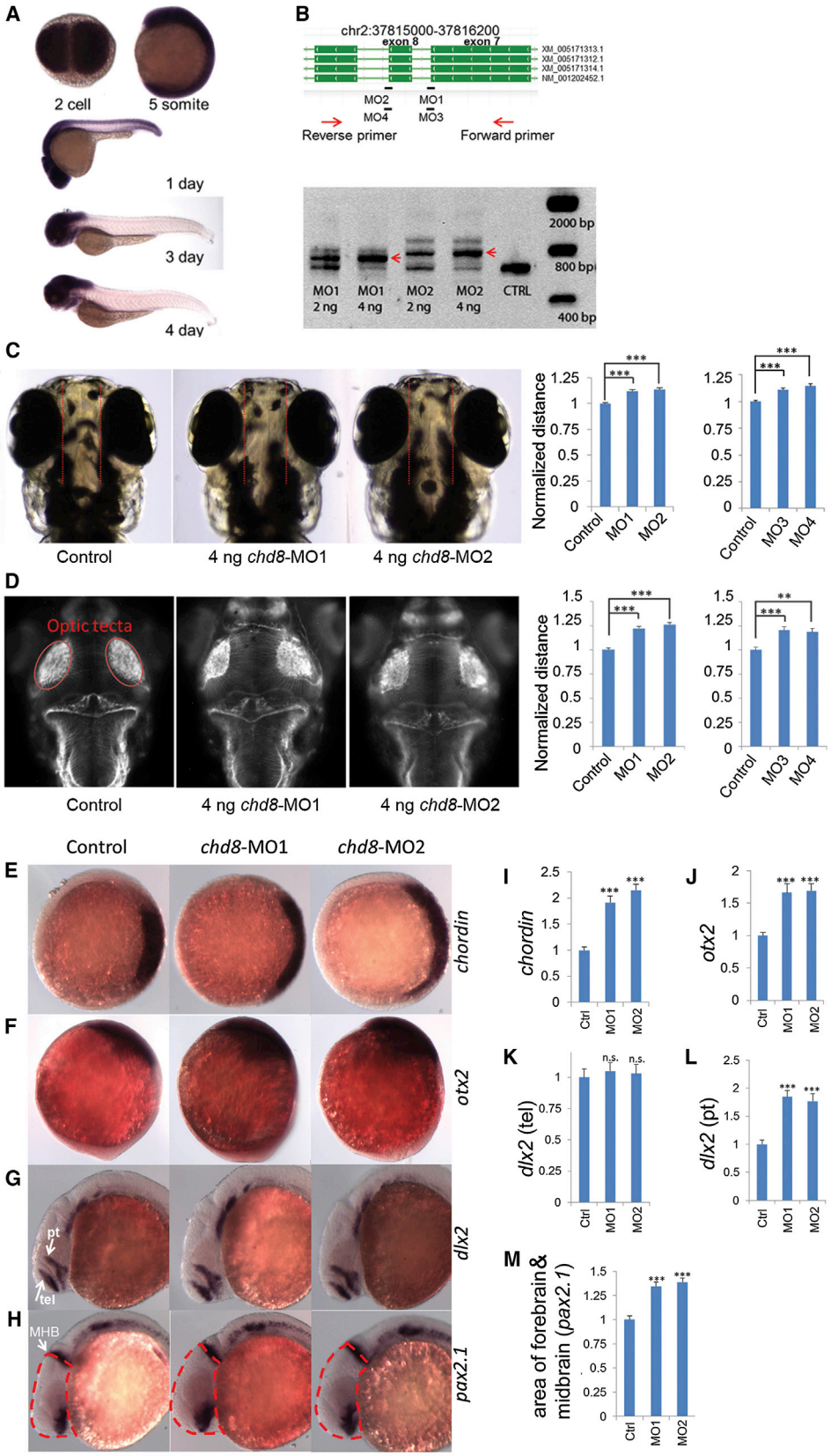

(legend on next page)

conserved between zebrafish and human (Figure S4A), we utilized zebrafish as a model system to suppress endogenous *chd8* and asked whether this alters the development of the brain and recapitulates some aspects of the human phenotype.

First, we generated two splice-blocking morpholinos (MO1 and MO2) targeting two exon-intron junctions of the zebrafish ortholog of *chd8* (Figure 4B). RT-PCR and Sanger sequencing confirmed that the morpholino design reduces normal splicing by >80%, leading to the inclusion of an intron adjacent to two different exons and a concomitant disruption of the Chd8 protein at aa604 and aa643 (Figure 4B). To examine the consequence of *chd8* disruption in head development, we first measured the distance between the convex tips of the eyes (interorbital distance) at ~4.3 dpf as a surrogate measurement for head size (Golzio et al., 2012). Injection of 4 ng of MO1 or MO2 leads to a significant increase in the mean value of the eye distances of 50 morphants ($p < 0.0001$), suggesting an overgrowth of the head (Figure 4C). Importantly, this phenotype was not accompanied by gross developmental abnormalities; MO-injected embryos developed their swim bladder appropriately (data not shown), and we did not identify significant changes in body length (Figure S4B) or length between somites (Figure S4C) compared to controls.

To determine whether larger head size was accompanied by increased brain volume in *chd8* morphants, we performed immunostaining with antiacetylated tubulin (used to label axonal tracts) on MO1- and MO2-injected embryos, which showed a significant increase in the mean distance between optic tecta compared to controls ($p < 0.0001$; Figure 4D). These observations were further supported by marker analysis using in situ hybridization of wild-type, MO1-, or MO2-injected embryos. At the shield stage, *chd8* morphants exhibited expansion of the dorsal organizer marked by *chordin*, suggesting that disruption of *chd8* promotes dorsal (neuronal) development (Figures 4E and 4I). At the tail bud stage, expression of *otx2*, an early marker of midbrain/forebrain neuronal progenitors, was upregulated in *chd8* morphants, consistent with its role in neuronal development (Figures 4F and 4J). At 24 hr postfertilization (hpf), we observed a significant increase of *dlx2* staining in the prethalamus, but not the telencephalon (Figures 4G, 4K, and 4L). In addition, we measured the size of the head region that contains the forebrain and midbrain marked by *pax2.1* staining and observed an enlargement of the forebrain/midbrain region (Figures 4H and 4M). In contrast, we did not observe significant changes to the markers of the telencephalon/eye (*pax6*) and hindbrain (*krox20*) (Figure S6).

Although macrocephaly is not a typical side effect of MO toxicity, we wanted to probe further the specificity of our results. The large size of the full-length human *CHD8* mRNA rendered it intractable to adequate in vitro transcription to perform rescue experiments, and we therefore carried out a series of additional experiments. First, we determined that the head size defect was dose dependent (Figure S4D). We designed two additional nonoverlapping splice-blocking MOs (MO3, MO4) that disrupted the splice donor site of exons 7 and 8, respectively, as determined by RT-PCR (Figures 4B and S4E). Injection with either MO reproduced the macrocephalic phenotype (Figures 4C and 4D). As a final test of specificity of the phenotype, we induced microdeletions in exon 2 of *chd8* by the clustered regularly interspaced short palindromic repeats (CRISPR)/Cas9 system (Hwang et al., 2013; Jao et al., 2013) (Figure S5A) and validated the presence of genetic editing in 50% of the injected embryos (founders, F0) by T7 endonuclease I assay (Figure S5B) and by single-molecule, real-time (SMRT) DNA sequencing (Figure S5C). We designed guide mRNAs against both *chd8* and the gene *tyr* (encoding tyrosinase), mutations that induce loss of pigmentation (Jao et al., 2013). Injections of guide RNAs and in-vitro-transcribed, capped, polyadenylated *nls-zCas9-nls* RNA into one-cell stage embryos, performed in duplicate by two

Figure 4. *chd8* Disruption Results in Ectopic Expression of Forebrain/Midbrain Markers during Zebrafish Development

In situ hybridization is shown for multiple markers before and after injection of *chd8*-MO1-4.

(A) In situ hybridization of 2-cell, 5-somite, 1-, 3-, and 4-day stage zebrafish embryos using a 1.5 kbp *chd8* antisense probe. *chd8* is ubiquitously expressed in early stages; however, after day 1, its expression is enriched in the head region and the GI duct.

(B) Two sets of morpholinos are independently designed to target two exon/intron junctions of *chd8*. To validate the morpholino effects, total mRNA was extracted at 24 hr postfertilization (hpf) followed by reverse transcription and PCR using primers flanking the targeted junctions. MO1 or MO2 injection leads to inclusion of the adjacent intron to mature mRNA. Red arrows indicate the PCR products of morpholino-modified *chd8* transcripts. Uninjected AB strain embryos were used as control for all experiments in Figure 4. Data are represented as mean ± SEM.

(C) The distance between the convex tips of the eyes was measured. MO1, MO2, MO3, and MO4 injection caused enlargement of this distance, and the results were quantified in the right panel. Data are represented as mean ± SEM.

(D) Embryos were immunostained to highlight the neuronal axon tract in the developing brains. Embryos are imaged in dorsal view, and the optic tecta structure is indicated (red oval). The average distance between the optic tecta is measured and quantified (n = 50). Injection of *chd8*-MO1, MO2, MO3, and MO4 showed an enlargement of the distance consistent with interorbital distance measurements. Data are represented as mean ± SEM.

(E and F) (E) Expression of *chordin* (marker of the dorsal organizing region) at shield stage, animal pole view, and dorsal oriented toward right. *Chordin* expression is expanded upon injection of *chd8* morpholinos, and the overall staining intensity is quantified. (F) Orthodenticle homeobox 2 (*otx2*), an early marker of midbrain and forebrain neuronal progenitors. Expression of *otx2* at tail bud stage, lateral view and dorsal oriented toward the right. *Otx2* expression is enhanced upon injection of *chd8* morpholinos and the overall staining intensity is quantified.

(G and H) (G) Distal-less homeobox 2 (*dlx2*), a marker of neural stem cells. Expression of *dlx2* at 24 hr stage, lateral view. Arrows point at the telencephalon (tel) region, and arrowhead points at the prethalamus (pt) region. *dlx2* expression in the prethalamus, but not telencephalon, region is enhanced upon injection of *chd8* morpholinos, as shown in (H) (pt) and (G) (tel), respectively. (H) Paired-box 2.1 (*pax2.1*), a marker of the midbrain/hindbrain boundary (MHB). Expression of *pax2.1* at 24 hr stage, lateral view. Arrow points at MHB. The area of the head that contains the forebrain and midbrain is outlined by dashed red lines. The forebrain/midbrain region is enlarged upon injection of *chd8* morpholinos, which is quantified.

(I–M) Quantification of significant in situ hybridization results. n.s., not significant; **$p < 0.001$; ***$p < 0.0001$. Data are represented as mean ± SEM.

See also Figures S4, S5, and S6.

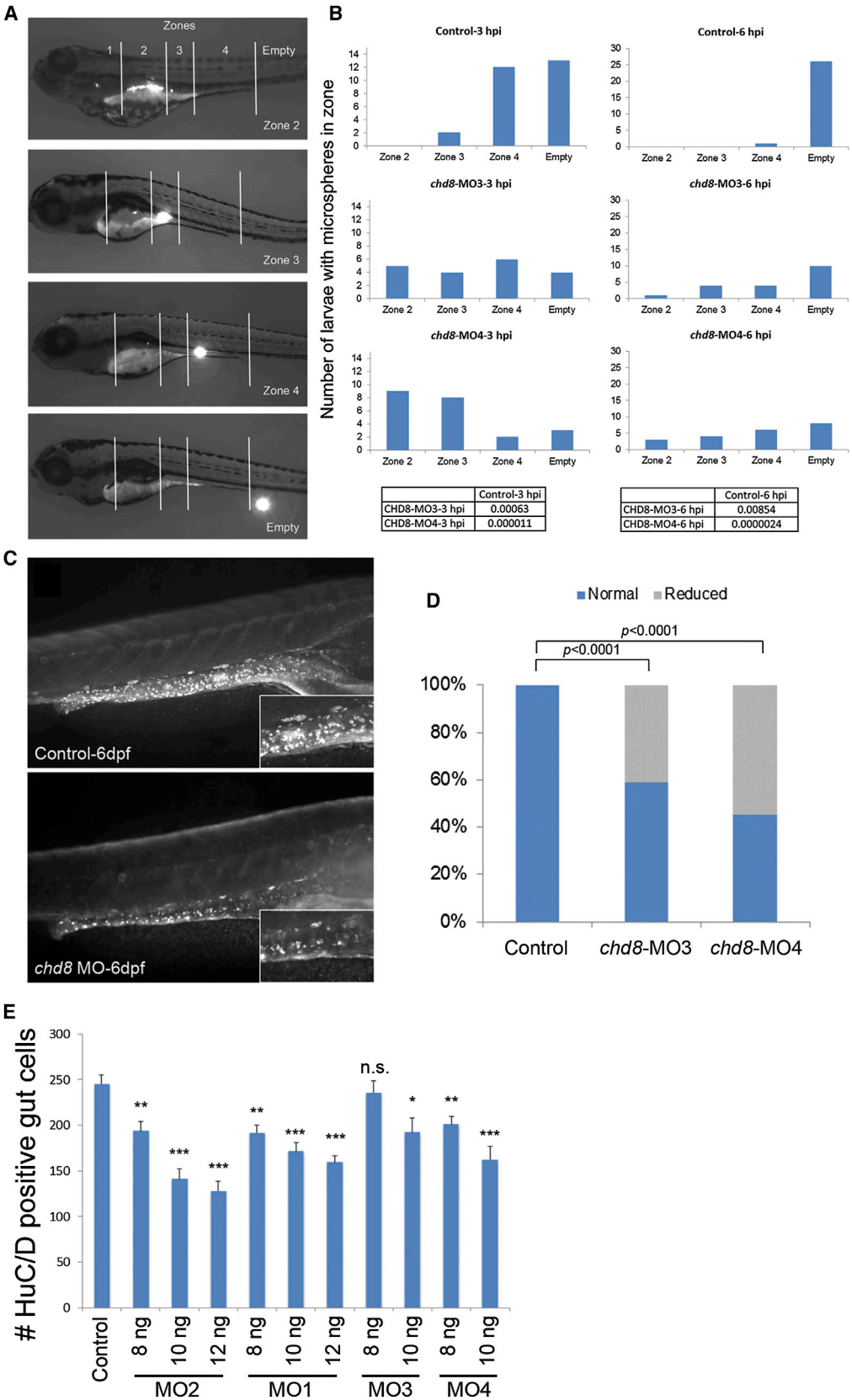

(legend on next page)

investigators, followed by phenotyping at 5 dpf blind to injection cocktail not only produced mosaic hypopigmentation phenotypes in 70% and 80% of the embryos in the two clutches, respectively, but also reproduced the head size defect seen with all four *chd8* MOs ($p < 0.0001$); objective measurement of interorbital distance in 70 CRISPR/Cas9-injected embryos and 32 sham-injected controls showed a mean increase of 17% in each clutch (Figures S5D and S5E). We note that we cannot determine how many cells carried Cas-9-induced *chd8* small insertions-deletions (indels) in each embryo nor whether the mutated cells were homozygous or heterozygous. However, we have not observed any homozygous *CHD8* mutations in human patients, which is consistent with the embryonic lethality observed in mouse knockout models of *Chd8* (Nishiyama et al., 2012). More importantly, the consistency of the phenotype of the injected animals with the humans carrying *CHD8* mutations and with the morpholino knockdowns and the lack of such phenotypes in our controls (the guide RNA that did not yield *chd8* mutations and the *tyr* mutants) supports the interpretation that loss of function of *CHD8* causes macrocephaly. These data are consistent with the macrocephaly and hypertelorism symptoms observed in patients, providing further evidence that *CHD8* plays a conserved role in regulating brain growth during development in both humans and zebrafish.

Because of the frequent GI complaints reported in patients with disruptive *CHD8* mutations, we also examined possible effects of *chd8* disruption during hindgut development. To test whether suppression of *chd8* affects GI motility, we performed an established microgavage assay (Cocchiaro and Rawls, 2013). We gavaged sham-, *chd8* MO3-, and MO4-injected larvae ($n = 25$) by injecting fluorescent microspheres into the intestinal anterior bulb and tracking the movement of the microspheres at different time points postgavage. We evaluated GI motility by defining four transit zones along the GI tract (Field et al., 2009) and scoring the more rostral location of the microspheres in live larvae at 3 and 6 hr postgavage (Figure 5A). Scoring blind to injection cocktail, we observed a significant delay of progression of the microspheres along the GI tract in both *chd8* morphants (MO3 and MO4) compared to sham-injected embryos at 3 hr postgavage (Figure 5B). Strikingly, whereas sham-injected embryos had no appreciable beads in zone 2 at 3 hr postgavage, 5/19 and 9/21 embryos injected with MO3 and MO4, respectively, had microspheres in zone 2 ($p = 6.3 \times 10^{-4}$ and $p = 1.1 \times 10^{-5}$ for *chd8*-MO3 and *chd8*-MO4, respectively; Figure 5B). The decrease of motility was still prominent after 6 hr; whereas 26/27 sham-injected embryos had no microsphere in zones 2–4, 9/19 and 13/21 MO-injected embryos had microspheres in zones 2–4 ($p = 0.00854$ and $p = 2.4 \times 10^{-6}$ for *chd8*-MO3 and *chd8*-MO4, respectively; Figure 5B).

GI motility is controlled by enteric neurons—neural crest-derived cells that form the enteric nervous system and undergo extensive migration from the caudal hindbrain to colonize the entire GI tract (Ciment and Weston, 1983). To investigate the cause of motility defects observed in the *chd8* morphants, we tested whether the disruption of *chd8* might affect the neuronal colonization of the GI tract. We stained embryos injected with MO3 or MO4 with an anti-HuC/D monoclonal antibody, a marker for postmitotic neurons; previous studies showed that enteric neurons are positive for both HuC and HuD (also known as *ELAVL3* and *ELAVL4*; D'Autréaux et al., 2007). Masked qualitative scoring of MO-injected embryos at 6 dpf (60 larvae per condition, repeated three times and scored blind by two investigators) showed that 40%–60% of embryos had a reduced number of HuC/D+ cells compared to controls ($p < 0.0001$; Figures 5C and 5D). Further, we performed a quantitative scoring by counting the number of enteric neurons that colonized the hindgut in a subset of morphants and controls (20 larvae per condition); we observed a mean of 144 HuC/D+ cells in the morphants compared to a mean of 278 in controls ($p = 0.0026$), indicating an average of 50% reduction of the number of enteric neurons present in the hindgut in *chd8* morphants compared to controls. Similar to our observations for head size, this phenotype could be both exacerbated in an MO dose-dependent manner and reproduced by MO1 and MO2 (Figure 5E), providing evidence of specificity. Finally, staining of our CRISPR-*chd8* embryos (scored live for head size and pigmentation defects) showed a significant reduction of enteric neurons ($p < 0.0002$; Figures S5F & S5G). Taken together, our data suggest that GI problems (constipation episodes followed by loose stool) in our patients with *CHD8*-truncating mutations are likely due, at least in part, to a reduced colonization of the GI tract by enteric neurons, which is expected to result in compromised motility.

Figure 5. Analysis of GI Motility by Microgavage Assay

(A) Example of intestinal transit within one larva over time. Intestinal zones are indicated in the top image (zones 1–4). Images below show fluorescent signal in the different intestinal zones outlined by white solid lines.

(B) The most rostral location of microspheres was used to determine the transit zone scores. Bars represent the total number of larvae containing microspheres in each zone, and numbers at the top of each graph indicate the time elapsed after gavage (hours postinjection [hpi]). Numbers of larvae injected and scored are as follow: 27 sham-injected, 19 *chd8*-MO3-injected, and 22 *chd8*-MO4-injected. The microgavage experiment was repeated three times. Fisher's exact test was performed; associated p values are shown in the corresponding tables.

(C) Injection of *chd8*-MO leads to a reduced number of enteric neurons in the GI tract at 6 days postfertilization (dpf). Representative photographs (with HuC/D-antibody staining) show the lateral views of a sham-injected zebrafish larva (control) and a zebrafish larva injected with *chd8* MO. Higher magnification of the GI tract, displayed in the insets, shows a reduced number of enteric neurons (labeled by anti-HuC/D antibody) in larvae injected with *chd8* MOs compared to controls.

(D) The bar graph represents the percentage of larvae (controls and injected with *chd8*-MO3 and -MO4) with reduced number of enteric neurons at 6 dpf. Corresponding p values are denoted on the bar graph (Pearson's chi-square test).

(E) Increasing the dosage of MO1-2 injection from 8 to 12 ng and MO3-4 from 8 to 10 ng resulted in a significant decrease in enteric neurons in the gut at 6 dpf measured by HuC/D-positive cells. n.s., not significant; *$p < 0.05$; **$p < 0.001$; ***$p < 0.0001$ (Student's t test). Data are represented as mean ± SEM.

See also Figures S4 and S5.

DISCUSSION

Our findings suggest that *CHD8* disruptions represent a specific pathway in the development of ASD and define a distinct ASD subtype. Common phenotypic features include increased head size accompanied by rapid, early postnatal growth; a facial phenotype marked by prominent forehead, wide-set eyes, and pointed chin; as well as increased rates of GI complaints and marked sleep dysfunction. Of these, the facial features, macrocephaly, and GI complaints (constipation) appear most significant when compared to other ASD patients without *CHD8* mutations. This association between macrocephaly and ASD is not the first to be reported in genetically defined subgroups. Mutations in *PTEN* are associated with severe macrocephaly and ASD (Butler et al., 2005), as is the 16p11.2 deletion CNV, modeled subsequently in zebrafish embryos with dosage changes in *KCTD13* (Golzio et al., 2012). We propose that this constellation of symptoms is particular to this genetically defined subtype of ASD irrespective of differences in the genetic background. The specificity of the ASD diagnosis is also noteworthy in light of the fact that our screen of more broadly defined developmental delay patients recovered four patients, of which three could be subsequently clinically classified with ASD. Most truncating mutations are de novo and associated with ASD, with no truncating mutations observed in 8,792 controls. These findings are consistent with *CHD8* mutations associating strongly with autism (OR = Inf, 95% C.I. = 4.35-Inf). Other events strongly associated with ASD, such as CNVs at 16p11.2 (Weiss et al., 2008), when ascertained more broadly (e.g., Simons Vip Consortium, 2012), reveal significant variability in clinical phenotype.

This study represents a realization of the genotype-first approach applied to ASD (Hennekam and Biesecker, 2012; Schulze and McMahon, 2004; Stessman et al., 2014). Although it required targeted resequencing of 6,176 patients with autism and developmental delay to recover 15 patients with severe truncating mutations, the clinical recontact and detailed characterization of this small subset was critical. Recognition of these specific but otherwise subtle phenotypes would have been obscured in an ASD clinic, where patients with diverse genetic and nongenetic etiologies present. Patients linked by a common genetic etiology may provide a superior classifier in distinguishing subtypes of the disease. It is also possible that a larger cohort of *CHD8* patients studied longitudinally will reveal additional features. We note, for example, that one of the female patients presented with precocious puberty, macrocephaly, and intellectual disability mirroring the phenotype of a translocation patient described earlier (Talkowski et al., 2012). Similarly, we note that both of our patients over the age of 40 developed tumors. In particular, the father of patient Nij07-06646 died from complications of metastases of a rectum carcinoma diagnosed at age 42. *CHD8* has been shown to play a role in the cell cycle of gastric cancer and has been associated with ten different gastric/colorectal cancers (Kim et al., 2011). Reduced *CHD8* expression observed in cancer tissues relative to healthy tissues from samples of 101 patients with gastric cancer and additional disruption of *CHD8* expression resulted in increased proliferation of cancer cell lines, suggesting that the loss of *CHD8* expression may be a novel indicator for gastric cancer (Sawada et al., 2013). This suggests that it may be important to study the *CHD8* ASD cohort longitudinally for early signs of colorectal cancer.

Several lines of evidence indicate that disruption of *CHD8* leads to defects in normal neuronal development. In multiple species, the developing brain shows the highest level of expression before birth. In humans, postmitotic layers of the neocortex show peak expression during midfetal development (15–16 pcw). At 21 pcw, a more significant increase in expression is observed for the ventricular and subventricular zone layers, which include a large proportion of neuronal precursors. Morphant *chd8* zebrafish recapitulate the macrocephaly phenotype (10%–15% enlargement) and a GI motility defect reminiscent of the gut motility defects found in patients. Importantly, these phenotypes were not accompanied by an overall advance or delay in *chd8* morphant embryonic development, suggesting specificity. Marker analyses of early embryonic neuronal development indicated that the head overgrowth is mostly driven by forebrain/midbrain expansion, which is likely due to overproliferation of neuronal progenitors of these regions. It is noteworthy that, in the forebrain region, *dlx2* expression is enhanced in the prethalamus, but not in the telencephalon in *chd8* morphants, suggesting that the overgrowth phenotype is highly tissue specific. Antibody staining indicates a reduction of enteric neurons in these morphants, suggesting a defect in either proliferation or colonization of the neural plexus during development. These findings are consistent with *CHD8*'s role as a master transcriptional regulator associated with cell proliferation and its relationship to other neurodevelopmental disorders, such as CHARGE syndrome (Vissers et al., 2004). CHARGE is an autosomal dominant syndrome marked by coloboma, heart defects, atresia of the choanae, retarded growth and development, genital hypoplasia, ear anomalies, and deafness (Hittner et al., 1979; Pagon et al., 1981). *CHD8* has been implicated previously in CHARGE syndrome through binding with *CHD7*, mutations to which are the major cause of CHARGE (Batsukh et al., 2010).

Finally, reproduction of the present paradigm for other genes associated with ASD, with particular emphasis on comorbidities, might represent an opportunity to stratify ASD into discrete clinical entities that can not only guide both diagnosis and management but can also inform the genotypic stratification of future clinical trials and provide nonbehavioral endpoints to test therapeutic efficacy.

EXPERIMENTAL PROCEDURES

Cohorts

DNA samples for cases with a diagnosis of ASD/developmental delay were obtained from six centers (Table S1). Post-MIP processing of 3,730 cases passed sequencing QC and were included in the analysis—these include 876 cases (two cohorts) with a diagnosis of ASD and 2,854 cases (four cohorts) with a general diagnosis of developmental delay/intellectual disability. In addition, we sequenced 2,289 siblings from the SSC as a control population.

MIPs and Sequence Analysis

Blood samples were collected and genomic DNA was isolated as part of participation in previous genetic studies of ASD (SSC; Fischbach and Lord, 2010) or developmental delay/intellectual disability. MIPs were designed as

described in O'Roak et al. (2012a). In total, 105 overlapping probes covering the coding sequence and splice junctions were included in the assay as part of a larger set of probes (O'Roak et al., 2012a). MIP Illumina HiSeq-based sequencing and analysis were performed as previously described (O'Roak et al., 2012a). Samples were included in the analysis if ≥90 of 105 *CHD8* probes demonstrated read depth over 20. All MIP screening was performed on probands, and putative disruptive variants in *CHD8* were validated by Sanger sequencing. Postvalidation, parental DNA were acquired and screened by Sanger sequencing for inheritance. Inspection of splice-site variants was performed using Alamut (Interactive Biosoftware), which incorporates five common splice prediction algorithms (SpliceSiteFinder-like, MaxEntScan, GeneSplicer, NNSPLICE, and Human Splicing Finder). For each splice site, we calculated the percent difference between the wild-type and variant sequence scores and averaged the results across the five algorithms.

Patient Assessment

Patients were initially identified through exome and targeted sequencing in anonymized ASD or developmental delay cohorts. Approval to initiate recontact of these identified patients for comprehensive phenotypic workup was obtained through the institutional review boards (IRBs) for each of the patient cohorts. The study team contacted the patient coordinators involved in the original studies to indicate which patients should be recontacted. The patient coordinators then decoded the sample IDs and recontacted families for comprehensive phenotypic workup. This included obtaining informed consent, coordinating travel to the clinical site, standardized examination of the neurocognitive and physical phenotype, and comprehensive medical records review (University of Washington IRB protocol HSD#42744).

Array Comparative Genomic Hybridization

To confirm rare CNVs in *CHD8*, we utilized a custom Agilent 8 × 60K comparative genomic hybridization (CGH) array with 150 bp probe spacing across the gene body of *CHD8* and predicted neighboring regulatory elements. In addition, large genomic CNVs were identified using a previously described Agilent 2 × 400K array (Girirajan et al., 2013).

Expression Analyses

The spatiotemporal pattern of expression of *CHD8* for human, macaque, and mouse was assessed using RNA-seq and microarray data available from the Allen Institute for Brain Science (http://www.brainmap.org/). Genes were assessed for correlated expression using RNA-seq data for all brain tissues available from the BrainSpan Atlas (http://www.brainspan.org/). These data provide high spatial and temporal resolution of genome-wide transcriptional changes in the human brain from 8 pcw through adulthood. Positive correlations in gene expression were assessed at various thresholds (Pearson correlation), and significance with respect to autism was established using a two-tailed Fisher's exact test.

Zebrafish Morpholino, In Situ Hybridization, Immunostaining, and Embryo Manipulations

Zebrafish (*Danio rerio*) embryos were raised and maintained as previously described (Westerfield, 1995), and the AB strain was used as wild-type for this study. Whole-mount in situ hybridization was performed as previously described (Thisse et al., 1993), and NBT/BCIP (Roche) was used as the chromogenic substrate. For *chd8* expression, digoxigenin-labeled RNA antisense probes were generated from ~1.5 kbp segments of *chd8* cloned into PCR4-TOPO vector (Invitrogen). To quantify staining, we used ImageJ. We first cycled the stained area with the "freehand selection" tool and measured the overall intensity using the "Measure" function. We then moved the shape to an unstained area to measure the background intensity. Finally, we subtracted the background intensity to get the actual staining intensity. We measured 25 stained embryos for each marker to obtain the average value.

Antisense morpholino oligonucleotides (GeneTools) were injected into 1–2 cell stage embryos. Two sets of morpholinos against *chd8* were designed separately. MO1/MO3 target the splice donor site of exon 7, and MO2/MO4 target the splice donor site of exon 8. Morpholino sequence: *chd8*-MO1, 5′-AATGGAATCATAACTTACTTGAGCT-3′; *chd8*-MO2, 5′-ATGTGCAAGCAAGTAACACCTGTGA-3′; splice-blocking MOs against *chd8*: (*chd8*-MO3, 5′- GAGAATGGAATCATAACTTA CTTGA-3′ and *chd8*-MO4, 5′- GCAAATGTGCAAGCAAGTAACACCT-3′. The two sets of overlapping morpholinos were designed independently by two different groups. Suppression of endogenous message was shown by PCR amplification of cDNA reverse transcribed from extracted total mRNA. To measure the interorbital distance, images of the embryo heads were taken around 4.3 dpf and were then analyzed using ImageJ; 50 embryos were measured for each genotype. Measurements of distance between five consecutive chevrons as a readout for body length was performed at 5 dpf as described (Golzio et al., 2012).

Whole-mount immunostaining with the antiacetylated tubulin (T7451, Sigma) or anti-HuC/D (A-21271, Life Technologies) was performed to examine the axon tract in the brain or enteric neurons along the GI tracts, respectively. Embryos were fixed in Dent's fixative (80% methanol, 20% dimethylsulphoxide [DMSO]) overnight. After rehydration with decreasing series of methanol in PBS, the embryos were washed with PBS, permeabilized with 10 μg/ml proteinase K, and postfixed with 4% PFA. Embryos were then washed twice with IF buffer (0.1% Tween-20, 1% BSA in 1 × PBS) for 10 min at room temperature. After incubation in blocking solution (10% FBS, 1% BSA in 1 × PBS) for 1 hr at room temperature, embryos were incubated with the antiacetylated tubulin (1:500) or anti-HuC/D antibody (1:500) in blocking solution overnight at 4°C. After two washes in IF buffer for 10 min each, embryos were incubated in the secondary antibody solution, 1:1,000 Alexa Fluor rabbit anti-mouse IgG (A11001, Life Technologies), in blocking solution for 1 hr at room temperature. For acetylated tubulin staining, embryos were stained 4.3 dpf. The distance between the optic tecta was quantified using ImageJ. For HuC/D staining, injected embryos were stained at 6 dpf and classified into two groups, normal and affected, based on the absence or presence of enteric neurons compared with an age-matched control group from the same clutch. Number of HuC/D-positive cells in the gut at 6 dpf was then quantified using ITCN (Image-based Tool for Counting Nuclei) plugin in ImageJ. All of the experiments were repeated three times.

Microgavage of Zebrafish Larvae

Sham-injected and *chd8* MO-injected zebrafish larvae were gavaged at 6 dpf with a suspension of 0.25% fluorescent microspheres/1 × PBS/0.05% phenol red as described previously (Field et al., 2009). Microsphere transit through the intestine was followed by live stereomicroscopy at 3 and 6 hr postgavage. Larvae were scored based on the location of the microspheres in intestinal zones (1–4) at the time points postgavage. The gavage experiment was repeated three times.

SUPPLEMENTAL INFORMATION

Supplemental Information includes Extended Experimental Procedures, six figures, and five tables and can be found with this article online at http://dx.doi.org/10.1016/j.cell.2014.06.017.

AUTHOR CONTRIBUTIONS

R.B. conducted initial clinical recontact. C.G., B.X., and L.F. performed zebrafish experiments. H.A.S. performed gene expression analysis. B.P.C. performed genotyping experiments. These authors contributed equally to the manuscript. N.K. and E.E.E. supervised all genotyping and zebrafish experiments. All authors discussed the results and commented on the manuscript at all stages.

ACKNOWLEDGMENTS

This work was supported by the Simons Foundation Autism Research Initiative (SFARI) 303241 and NIH/NIMH R01MH101221 to E.E.E.; by SFARI 239983 and NIH P50MH094268 to N.K.; by a NARSAD Young Investigator Grant from BBRF to C.G.; and by the European Commission: GENCODYS grant 241995 under FP7 and the Dutch Organisation for Health Research and Development (ZON-MW grants 917-86-319 and 912-12-109) to B.B.A.d.V. E.E.E. is an Investigator of the Howard Hughes Medical Institute and is on the scientific advisory board for DNAnexus, Inc. N.K. is a Distinguished Brumley Professor.

We thank all of the families at the participating Simons Simplex Collection (SSC) sites, as well as the principal investigators (A. Beaudet, R. Bernier, J. Constantino, E. Cook, E. Fombonne, D. Geschwind, E. Hanson, D. Grice, A. Klin, R. Kochel, D. Ledbetter, C. Lord, C. Martin, D. Martin, R. Maxim, J. Miles, O. Ousley, K. Pelphrey, B. Peterson, J. Piggot, C. Saulnier, M. State, W. Stone, J. Sutcliffe, C. Walsh, Z. Warren, and E. Wijsman). We are grateful to D. Raible and H.S. Zimmermann for providing zebrafish resources and for helpful discussions, to T. Brown for help with manuscript preparation, and to J. Huddleston and M. Malig for sequencing support.

Received: January 29, 2014
Revised: May 1, 2014
Accepted: June 5, 2014
Published: July 3, 2014

REFERENCES

American Psychiatric Association (2000). Diagnostic and Statistical Manual of Mental Disorders, Fourth Edition, Text Revision (DSM-IV-TR) (Washington, DC: American Psychiatric Association).

American Psychiatric Association (2013). Diagnostic and Statistical Manual of Mental Disorders, Fifth Edition (DSM-5) (Washington, DC: American Psychiatric Association).

Batsukh, T., Pieper, L., Koszucka, A.M., von Velsen, N., Hoyer-Fender, S., Elbracht, M., Bergman, J.E., Hoefsloot, L.H., and Pauli, S. (2010). CHD8 interacts with CHD7, a protein which is mutated in CHARGE syndrome. Hum. Mol. Genet. *19*, 2858–2866.

Betancur, C. (2011). Etiological heterogeneity in autism spectrum disorders: more than 100 genetic and genomic disorders and still counting. Brain Res. *1380*, 42–77.

Butler, M.G., Dasouki, M.J., Zhou, X.P., Talebizadeh, Z., Brown, M., Takahashi, T.N., Miles, J.H., Wang, C.H., Stratton, R., Pilarski, R., and Eng, C. (2005). Subset of individuals with autism spectrum disorders and extreme macrocephaly associated with germline PTEN tumour suppressor gene mutations. J. Med. Genet. *42*, 318–321.

Chaste, P., Klei, L., Sanders, S.J., Murtha, M.T., Hus, V., Lowe, J.K., Willsey, A.J., Moreno-De-Luca, D., Yu, T.W., Fombonne, E., et al. (2013). Adjusting head circumference for covariates in autism: clinical correlates of a highly heritable continuous trait. Biol. Psychiatry *74*, 576–584.

Ciment, G., and Weston, J.A. (1983). Enteric neurogenesis by neural crest-derived branchial arch mesenchymal cells. Nature *305*, 424–427.

Cocchiaro, J.L., and Rawls, J.F. (2013). Microgavage of zebrafish larvae. J. Vis. Exp. *72*, e4434.

D'Autréaux, F., Morikawa, Y., Cserjesi, P., and Gershon, M.D. (2007). Hand2 is necessary for terminal differentiation of enteric neurons from crest-derived precursors but not for their migration into the gut or for formation of glia. Development *134*, 2237–2249.

Field, H.A., Kelley, K.A., Martell, L., Goldstein, A.M., and Serluca, F.C. (2009). Analysis of gastrointestinal physiology using a novel intestinal transit assay in zebrafish. Neurogastroenterol. Motil. *21*, 304–312.

Fischbach, G.D., and Lord, C. (2010). The Simons Simplex Collection: a resource for identification of autism genetic risk factors. Neuron *68*, 192–195.

Geschwind, D.H. (2009). Advances in autism. Annu. Rev. Med. *60*, 367–380.

Girirajan, S., Dennis, M.Y., Baker, C., Malig, M., Coe, B.P., Campbell, C.D., Mark, K., Vu, T.H., Alkan, C., Cheng, Z., et al. (2013). Refinement and discovery of new hotspots of copy-number variation associated with autism spectrum disorder. Am. J. Hum. Genet. *92*, 221–237.

Golzio, C., Willer, J., Talkowski, M.E., Oh, E.C., Taniguchi, Y., Jacquemont, S., Reymond, A., Sun, M., Sawa, A., Gusella, J.F., et al. (2012). KCTD13 is a major driver of mirrored neuroanatomical phenotypes of the 16p11.2 copy number variant. Nature *485*, 363–367.

Gotham, K., Pickles, A., and Lord, C. (2009). Standardizing ADOS scores for a measure of severity in autism spectrum disorders. J. Autism Dev. Disord. *39*, 693–705.

Gulsuner, S., Walsh, T., Watts, A.C., Lee, M.K., Thornton, A.M., Casadei, S., Rippey, C., Shahin, H., Nimgaonkar, V.L., Go, R.C., et al.; Consortium on the Genetics of Schizophrenia (COGS); PAARTNERS Study Group (2013). Spatial and temporal mapping of de novo mutations in schizophrenia to a fetal prefrontal cortical network. Cell *154*, 518–529.

Hennekam, R.C., and Biesecker, L.G. (2012). Next-generation sequencing demands next-generation phenotyping. Hum. Mutat. *33*, 884–886.

Hittner, H.M., Hirsch, N.J., Kreh, G.M., and Rudolph, A.J. (1979). Colobomatous microphthalmia, heart disease, hearing loss, and mental retardation—a syndrome. J. Pediatr. Ophthalmol. Strabismus *16*, 122–128.

Houdayer, C. (2011). In silico prediction of splice-affecting nucleotide variants. Methods Mol. Biol. *760*, 269–281.

Hwang, W.Y., Fu, Y., Reyon, D., Maeder, M.L., Tsai, S.Q., Sander, J.D., Peterson, R.T., Yeh, J.R., and Joung, J.K. (2013). Efficient genome editing in zebrafish using a CRISPR-Cas system. Nat. Biotechnol. *31*, 227–229.

Iossifov, I., Ronemus, M., Levy, D., Wang, Z., Hakker, I., Rosenbaum, J., Yamrom, B., Lee, Y.H., Narzisi, G., Leotta, A., et al. (2012). De novo gene disruptions in children on the autistic spectrum. Neuron *74*, 285–299.

Jao, L.E., Wente, S.R., and Chen, W. (2013). Efficient multiplex biallelic zebrafish genome editing using a CRISPR nuclease system. Proc. Natl. Acad. Sci. USA *110*, 13904–13909.

Jiang, Y.H., Yuen, R.K., Jin, X., Wang, M., Chen, N., Wu, X., Ju, J., Mei, J., Shi, Y., He, M., et al. (2013). Detection of clinically relevant genetic variants in autism spectrum disorder by whole-genome sequencing. Am. J. Hum. Genet. *93*, 249–263.

Kim, M.S., Chung, N.G., Kang, M.R., Yoo, N.J., and Lee, S.H. (2011). Genetic and expressional alterations of CHD genes in gastric and colorectal cancers. Histopathology *58*, 660–668.

Lord, C., Petkova, E., Hus, V., Gan, W., Lu, F., Martin, D.M., Ousley, O., Guy, L., Bernier, R., Gerdts, J., et al. (2012). A multisite study of the clinical diagnosis of different autism spectrum disorders. Arch. Gen. Psychiatry *69*, 306–313.

Neale, B.M., Kou, Y., Liu, L., Ma'ayan, A., Samocha, K.E., Sabo, A., Lin, C.F., Stevens, C., Wang, L.S., Makarov, V., et al. (2012). Patterns and rates of exonic de novo mutations in autism spectrum disorders. Nature *485*, 242–245.

Nishiyama, M., Skoultchi, A.I., and Nakayama, K.I. (2012). Histone H1 recruitment by CHD8 is essential for suppression of the Wnt-β-catenin signaling pathway. Mol. Cell. Biol. *32*, 501–512.

O'Roak, B.J., Vives, L., Fu, W., Egertson, J.D., Stanaway, I.B., Phelps, I.G., Carvill, G., Kumar, A., Lee, C., Ankenman, K., et al. (2012a). Multiplex targeted sequencing identifies recurrently mutated genes in autism spectrum disorders. Science *338*, 1619–1622.

O'Roak, B.J., Vives, L., Girirajan, S., Karakoc, E., Krumm, N., Coe, B.P., Levy, R., Ko, A., Lee, C., Smith, J.D., et al. (2012b). Sporadic autism exomes reveal a highly interconnected protein network of de novo mutations. Nature *485*, 246–250.

Pagon, R.A., Graham, J.M., Jr., Zonana, J., and Yong, S.L. (1981). Coloboma, congenital heart disease, and choanal atresia with multiple anomalies: CHARGE association. J. Pediatr. *99*, 223–227.

Rauch, A., Wieczorek, D., Graf, E., Wieland, T., Endele, S., Schwarzmayr, T., Albrecht, B., Bartholdi, D., Beygo, J., Di Donato, N., et al. (2012). Range of genetic mutations associated with severe non-syndromic sporadic intellectual disability: an exome sequencing study. Lancet *380*, 1674–1682.

Sanders, S.J., Murtha, M.T., Gupta, A.R., Murdoch, J.D., Raubeson, M.J., Willsey, A.J., Ercan-Sencicek, A.G., DiLullo, N.M., Parikshak, N.N., Stein, J.L., et al. (2012). De novo mutations revealed by whole-exome sequencing are strongly associated with autism. Nature *485*, 237–241.

Sawada, G., Ueo, H., Matsumura, T., Uchi, R., Ishibashi, M., Mima, K., Kurashige, J., Takahashi, Y., Akiyoshi, S., Sudo, T., et al. (2013). CHD8 is an independent prognostic indicator that regulates Wnt/β-catenin signaling and the cell cycle in gastric cancer. Oncol. Rep. *30*, 1137–1142.

Schulze, T.G., and McMahon, F.J. (2004). Defining the phenotype in human genetic studies: forward genetics and reverse phenotyping. Hum. Hered. *58*, 131–138.

Shen, E.H., Overly, C.C., and Jones, A.R. (2012). The Allen Human Brain Atlas: comprehensive gene expression mapping of the human brain. Trends Neurosci. *35*, 711–714.

Simon, J.M., Hacker, K.E., Singh, D., Brannon, A.R., Parker, J.S., Weiser, M., Ho, T.H., Kuan, P.F., Jonasch, E., Furey, T.S., et al. (2014). Variation in chromatin accessibility in human kidney cancer links H3K36 methyltransferase loss with widespread RNA processing defects. Genome Res. *24*, 241–250.

Simons Vip Consortium (2012). Simons Variation in Individuals Project (Simons VIP): a genetics-first approach to studying autism spectrum and related neurodevelopmental disorders. Neuron *73*, 1063–1067.

Stessman, H.A., Bernier, R., and Eichler, E.E. (2014). A genotype-first approach to defining the subtypes of a complex disease. Cell *156*, 872–877.

Talkowski, M.E., Rosenfeld, J.A., Blumenthal, I., Pillalamarri, V., Chiang, C., Heilbut, A., Ernst, C., Hanscom, C., Rossin, E., Lindgren, A.M., et al. (2012). Sequencing chromosomal abnormalities reveals neurodevelopmental loci that confer risk across diagnostic boundaries. Cell *149*, 525–537.

Thisse, C., Thisse, B., Schilling, T.F., and Postlethwait, J.H. (1993). Structure of the zebrafish snail1 gene and its expression in wild-type, spadetail and no tail mutant embryos. Development *119*, 1203–1215.

Thompson, B.A., Tremblay, V., Lin, G., and Bochar, D.A. (2008). CHD8 is an ATP-dependent chromatin remodeling factor that regulates beta-catenin target genes. Mol. Cell. Biol. *28*, 3894–3904.

Vissers, L.E., van Ravenswaaij, C.M., Admiraal, R., Hurst, J.A., de Vries, B.B., Janssen, I.M., van der Vliet, W.A., Huys, E.H., de Jong, P.J., Hamel, B.C., et al. (2004). Mutations in a new member of the chromodomain gene family cause CHARGE syndrome. Nat. Genet. *36*, 955–957.

Weiss, L.A., Shen, Y., Korn, J.M., Arking, D.E., Miller, D.T., Fossdal, R., Saemundsen, E., Stefansson, H., Ferreira, M.A., Green, T., et al.; Autism Consortium (2008). Association between microdeletion and microduplication at 16p11.2 and autism. N. Engl. J. Med. *358*, 667–675.

Westerfield, M. (1995). The Zebrafish Book. A Guide for the Laboratory Use of Zebrafish (Danio rerio), Third Edition (Eugene, OR: University of Oregon Press).

Wing, L., and Gould, J. (1979). Severe impairments of social interaction and associated abnormalities in children: epidemiology and classification. J. Autism Dev. Disord. *9*, 11–29.